Systematic Studies of Phase Relation and Thermodynamic Stability of Ln-Rh-O System for Catalysis and Electrochemical Devices

Preeti Gupta and Vinita

Department of Chemistry

D. D. U. Gorakhpur University, Gorakhpur, U.P., India

preeti17_nov@yahoo.com

Abstract: *Ln-Rh-O systems show potential interest in different catalytic applications. Phase diagram of these systems revealed that only LnRhO₃, an orthorhombic perovskite structure, has been found as stable ternary oxide. Employed solid-state electrochemical cell to determine the thermodynamic parameters of LnRhO₃ compounds from their binary oxides Rh₂O₃ and Ln₂O₃. Calcia stabilized and yttria stabilized zirconia has been used as solid electrolytes in these cells. Ternary phase relation for Ln-Rh-O systems is established using isothermal equilibration technique. Phase diagram of few Ln-Rh-O systems are computed with the help of supplementary data for other binary phases (Ln-Rh) from the literature and thermodynamic data for LnRhO₃ from experiment at high temperature. At 298.15 K, ΔH_f^0 and S^0 for LnRhO₃are calculated from its constituting elements. Thermodynamic data has been used to compute an oxygen potential – composition and three-dimensional chemical potential diagram for the system Ln-Rh-O.*

Keywords: Catalytic Applications

I. INTRODUCTION

Developments in materials science and engineering that have made a major impact in the last decade. These functional materials find application as sensors, actuators and modulators in different sectors such as automotive, aeronautics, electronics, machine-tools and domestic appliances. In addition, some of these materials are also used in catalysis and electrochemical devices such as batteries, chemical and bio-sensors, electrochromic devices, fuel cells and solar cells [1-5]. Fundamental and systematic phase relations and thermodynamic data are essential for designing new materials with tailored properties. In order to provide high accuracy data, new solid–state electrochemical cells are designed to produce high–temperature thermodynamic data.

Ternary oxides *Ln*RhO₃ containing lanthanide elements display catalytic [1], electrochemical [2, 3] and interesting magnetic [4,5] properties. Studies has revealed that LaRhO₃as an active catalyst for the hydroformylation of olefins and conversion of synthetic gas to linear alcohols [1]. Dysporsium rhodite (DyRhO₃) has semiconducting in nature. Its optical band gap falls within the solar spectrum and also has stability over a wide range of pH in aqueous solutions. Because of the mentioned properties, it haspotential use as cathode in photoelectrolysis of water [3,6]. At 2 K, GdRhO₃exhibit antiferromagnetic transition which has been revealed byspecific heat and magnetic measurements [7].

Looking to the significant importance of Lanthanide–rhodium–oxygen systems in different applications, phase relations in a series of systems, *Ln*-Rh-O (*Ln*= Dy, Gd,La, Ho, Tm, Sm,Nd, Yb, Ce and Pr) has been explored [6-15]. In the defined temperature range, thermodynamic properties of *Ln*RhO₃ have been determined by employing a solid-state electrochemical cell. The phase diagrams and thermodynamic data on *Ln*RhO₃ are significant for determining stability of the catalyst under various environments, evaluating catalyst-support interactions and in the designing of strategies forcatalyst regeneration.

II. EXPERIMENTAL

2.1 Preparation of Materials

All LnRhO$_3$has been prepared mixing of fine powders of Ln_2O_3 and Rh_2O_3 in equimolar ratio. They were ground in ethanol and dried. At 1373 K, they were pelletized for heat treatment under pure O$_2$gas for 48 h. Occasional grindings were done for several times. Further at 1573 K, reaction is completed by heating under flowing oxygen for48 h. X-ray diffraction (XRD) technique is used to verify the formation of orthorhodite. The detailed method of preparation of materials is discussed elsewhere [10].

2.2 Phase Equilibrium Studies at High Temperature

Phase relations in Ln-Rh-O systems (Ln = Ho, Tm,Sm and Nd) has been established by using isothermal equilibration technique [9-12]. Mixtures of pure metals and binary oxides were equilibrated at high temperature in order to explore the phase relations in the system Ln–Rh–O in liquid nitrogen. The phase identification were performed at room temperature. Various samples of oxides and metals/intermetallics were pelletized. Under vacuum, the equilibration of the samples took place in a closed system. Quartz ampules were used to keep the samples and were evacuated to 0.1 MPa pressure and further flame sealed. With the aim to start the reaction between oxide andmetals/intermetallics, samples were heated to 1373 K for ~8 h. It was then equilibrated for ~120 h at 1273 K. Additional heat treatment do not bring any significant change in the phase compositions of the samples. Thus, the attainment of equilibrium was assumed. Phase identification was done by X-ray diffraction, energy dispersive spectroscopy and optical and scanning electron microscopy techniques.

2.3 Electrochemical Studies

The solid-state electrochemical cell,

Pt-13% Rh, Rh + LnRhO$_3$ + Ln_2O_3 // (CaO) or (Y$_2$O$_3$) ZrO$_2$// Rh$_2$O$_3$+ Rh, Pt-13% Rh
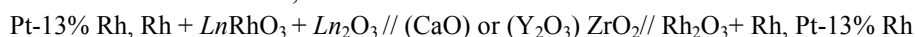
has been outlined. Measured reversible emf as a function of temperature in the range from 900 to 1300 K. Reference electrode (positive) on right-hand side and measuring electrodes on the left side. Both were separated by solid electrolyte i.e. a calcia–stabilized zirconia (CSZ) or Yttria stabilized zirconia (YSZ) tube. The predominant oxygen ion conduction (t$_{ion}$) is greater than 0.999 under the experimental conditions. Pt-13 % Rh alloy wires serve as electrical leads. Over the electrodes, there was appreciable partial pressure of oxygen at high temperatures. Thus, an evacuated and sealed system was used to contain the samples. Decomposition of Rh$_2$O$_3$ and DyRhO$_3$ created an oxygen partial pressure over both the electrodes. The electrochemical cells are designed in such a way that the EMF can be related to the Gibbs energy of formation of LnRhO$_3$ from component binary oxides Ln_2O_3 and Rh$_2$O$_3$. The detailed experimental description is given elsewhere [16]. The cell diagram is presented in Figure 1.

III. DISCUSSION

In the case of all nine Ln-Rh-O systems, the reversible emf of solid-state electrochemical cell has been measured and plotted against temperature from 900 to 1300 K. With the help of the oxygen potential of reference [17]and measuring electrodes, the oxygen potentials of LnRhO$_3$ are calculated by using the Nernst equation$\left(\Delta\mu_{O_2}^r - \Delta\mu_{O_2}^m = nFE\right)$.The standard Gibbs free energies of formation of O-type orthorhombic perovskites LnRhO$_3$ from the component binary oxides are obtained (Table 1). At 298.15 K, thermodynamic properties of LnRhO$_3$ can be calculated by using the Neumann-Kopp rule (Table 2).

The phase relation for the systems Ln-Rh-O are represented on the Gibbs' triangle. In Tm-Rh-Osystem, the relation is established at 1200, La at 1223 whereas in the case of Sm and Nd, it is at 1273 K. Three binary systems (Ln-Rh, Rh-O and Ln-O) forms the boundaries of the isothermal section of the ternary phase diagram.In all the systems, Rh-O and Ln-O binaries have only one oxide i.e. Rh$_2$O$_3$ and Ln_2O_3For the binary system Ln-Rh, various intermetallic compounds exist for all the four systems and are represented in Figure 2. Systems containa ternary oxide LnRhO$_3$with an orthorhombically distorted perovskite structure.LnRhO$_3$exists with Ln_2O_3, Rh$_2$O$_3$, Rh and O$_2$ in several phase fields.The

isothermal section for all the systems contains different three-phase regions and are represented in Table 3a. Figure 3 shows an isothermal section of Nd-Rh-O system at 1273 K.

With the help of thermodynamic information of all the three phases, phase diagram for the systems *Ln*-Rh-O (*Ln*= Dy, Gd, Ho, Yb, Ce and Pr) are generated. The Gibbs free energies of formation of Dy_2O_3, Gd_2O_3, Ho_2O_3, Yb_2O_3, Ce_2O_3 and Pr_2O_3 are taken from Pankratz [18]. In Ce-Rh-O ternary system, along Ce-O boundary, three non-stoichiometric compositions (Ce_2O_{3-x}, Ce_3O_{5+x}, CeO_{2-x}) and one stoichiometric phase (Ce_7O_{12}) are present at 1200K [14].Pr_2O_3 and Pr_7O_{12} are the two stable oxides at 1200 K in Pr-O binary system [15]. Thermodynamic informations for $LnRhO_3$are obtained from recent studies. Enthalpy of formation for various intermetallics are available in literature from calorimetric measurements [6-7,9,14-15]Free energies of formation of intermetallics are not measured. Thus, the values are estimated by using values for enthalpy of formation and Miedema's model[19] which are in consistent with the phase relation available in the literature[20]. Table 3b contains various three-phase regions for Ln-Rh-O which are computed from the literature data.

Oxygen potential diagrams for *Ln*-Rh-O (*Ln* = La, Ce, Pr, Nd, Sm, Dy, Gd, Ho) system at high temperature evaluated from thermodynamic data (Table 2). Figure 4 shows this diagram for Nd-Rh-O at 1273 K. This diagram implies that a gas phase and three condensed phases coexist at equilibrium in a ternary system. This clearly signifies that the system is univariant. At specific oxygen chemical potential and at constant temperature, three condensed phases can coexist. Horizontal lines on the diagram shows three-phase equilibria. The low oxygen potential region presents various intermetallic phases are in equilibrium with Nd_2O_3 and in the high oxygen potential region $NdRhO_3$ is in equilibrium with Nd_2O_3 or Rh_2O_3.Thisdiagram and Gibbs triangle diagram for ternary phase relation are complementary to each other (Figure 2).Similarly, oxygen potential diagrams for all other systems are explained in the literature [6-7, 9-12,14-15].

In this view, 3-D chemical potential diagram for Nd-Rh-O system at 1273 K is drawn and shown in Figure 5 [9]. Itexplicitly explains the stability domains of various phases in the chemical potential space. At fixed temperature, these stability domains of a ternary phasesarethe function of chemical potentials of the three components. An isothermal three- dimensional chemical potential diagram constitutes of three orthogonal axis which represent the chemical potential of each component. The stability domain of each stoichiometric phase is outlined by a plane and the stoichiometry of compound defines slope of plane. The non-stoichiometry in the composition is represented by a curved surface.Due to use of compressed scales, the curvature is evident in the figure. The intersection of adjacent planes forms a line which represent two-phase equilibria. Three phase equilibria in the diagram are presented by a point intersecting the three planes.Considering the binary compound, slope is infinite or zero in one direction. It is depicted from the figure that Nd_2O_3 is the dominant phaseand slopes are $(d\Delta\mu_{O_2}/d\Delta\mu_{Nd} = -1.333)$ and $(d\Delta\mu_{O_2}/d\Delta\mu_{Rh} = 0)$. At the lower oxygen potential axis, intermetallics are shown by vertical planes. Width of these planes measure the stability of these intermetallics. Plane at the right top corner represents $NdRhO_3$with high chemical potential of Rh and O_2 and low chemical potential of Nd. Slopes for$NdRhO_3$plane are $(d\Delta\mu_{O_2}/d\Delta\mu_{Rh} = -0.667)$ and $(d\Delta\mu_{O_2}/d\Delta\mu_{Nd} = -0.667)$. A plane representing the stability domain of Rh_2O_3place above that of the $NdRhO_3$. The plane for Rh_2O_3 is parallel to the $\Delta\mu_{Nd}$ axis and the slope is $(d\Delta\mu_{O_2}/d\Delta\mu_{Rh} = -1.333)$. The 3–D chemical potential diagram gives an explicit geometric image of the stability domains of various phases in the chemical potential space. The three-dimensional chemical potential diagrams for other system are explained in the same manner.

IV. CONCLUSION

Studies of phase relations impart the knowledge of phase stability and phase composition as a function of composition, pressure and temperature. They help in rationalizing synthetic procedures aimed at minimizing secondary phases that are usually present in complex oxides. They also allow to explore different processes such purifying, solidification, phase separation, sintering, and doping of single crystal for technological applications. It contributes in

predicting compositional changes, phase relations and structures in the systems, those are not in equilibrium. Along with this, thermodynamic studies provide information about how energy is stored, released and transferred in various processes. With the help of different thermodynamic parameters, one can evaluate the stability of phases.

REFERENCES

[1]. H.J. Gysling, J.R. Monnier, G. Apai, Synthesis, Characterization and catalysis of $LaRhO_3$, Journal of Catalysis, vol. 103, pp. 407–418, 1987.

[2]. W. Yi, Q. Liang, Y. Matsushita, M. Tanaka, H. Xiao, A.A. Belik, Crystal structure and properties of high-pressure-synthesized $BiRhO_3$, $LuRhO_3$, and $NdRhO_3$, Journal Solid State Chemistry, vol. 200, pp. 271–278, Jan 2013.

[3]. H. S. Jarrett, H.H.C. Kung, A.W. Sleight,"Photolysis of water using rhodate semiconductive electrodes" US Patent 4,144,147, (1979)

[4]. T. Taniguchi, W. Iizuka, Y. Nagata, T. Uchida, H. Samata, Magnetic properties of $RRhO_3$ (R=rare earth), Journal of Alloys and Compounds,vol. 350, pp. 24-29, Feb 2003.

[5]. H.S. Jarrett, A.W. Sleight, H. H. Kung, J.L. Gillson, Photoelectrochemical and solid-state properties of $LuRhO_3$, JournalApplied Physics, vol. 51, pp.3916, 1980.

[6]. K. T. Jacob, Preeti Gupta, Electrochemical determination of thermodynamic properties of $DyRhO_3$ and phase relations in the system Dy-Rh-O, Journal Soild State Electrochemistry, vol. 17, pp. 607-615, Oct 2013.

[7]. K. T. Jacob, A. K. Dhiman, Preeti Gupta, System Gd–Rh–O: Thermodynamics and phase relations, Journal of Alloys and Compound, vol. 546, pp. 185-191, Jan 2013.

[8]. K. T. Jacob, Y Waseda, Phase relations in the system La-Rh-0 and thermodynamic properties of $LaRhO_3$, Journal of American Ceramic Society, vol. 78, pp.440-44, Feb 1995.

[9]. K. T. Jacob, Juhi Sharma, Preeti Gupta, System Ho-Rh-O: Phase equilibria, chemical potentials and gibbs energy of formation of $HoRhO_3$, Journal of Phase Equilibria and Diffusion, vol. 33, pp. 429-436, Sept 2012.

[10]. K. T. Jacob, Karuna Agarawal, Preeti Gupta, Thermodynamics of $TmRhO_3$, phase equilibria, and chemical potentials in the system Tm−Rh−O, Journal of Chemical and Engineering Data, vol. 57,pp. 3677-3684, Nov (2012).

[11]. K. T. Jacob, Preeti Gupta, Donglin Han, Tetsyu Uda, Phase equilibria in the system Sm–Rh–O and thermodynamic and thermal studies on $SmRhO_3$, Journal of Material Science, vol. 49, pp. 3135-3145, Jan (2014).

[12]. K. T. Jacob, Preeti Gupta, Donglin Han, Tetsyu Uda, Thermodynamics of $NdRhO_3$ and phase relations in the system Nd–Rh–O, CALPHAD, vol. 43, pp. 71-79, Dec (2013).

[13]. K. T. Jacob, Preeti Gupta, Donglin Han, Tetsyu Uda, Thermodynamic properties of $YbRhO_3$ and phase relations in the system Yb-Rh-O, Journal of Phase Equilibria and Diffusion, vol. 37, pp. 503-509, June (2016).

[14]. K.T. Jacob, S. Muraleedharan Phase diagram of the system Ce-Rh-O, Calphad, vol 65, pp 171-176, June 2019,

[15]. K.T. Jacob, S. Muraleedharan, Thermodynamic properties of $PrRhO_3$ and phase diagrams of the system Pr–Rh–O, Journal of American Ceramic Society, vol 102, pp. 7617-7627, Dec 2019.

[16]. K.T. Jacob, C. Shekhar, Waseda Y Phase relations in the system Ta–Rh–O and thermodynamic properties of $TaRhO_4$, Materials Chemistry and Physics, vol. 116, pp. 289-293, July 2009.

[17]. . K.T.Jacob, M.V.Sriram. Phase relations and Gibbs energies in the system Mn-Rh-O, Metallurgical Material Transaction A,vol. 25, pp 1347-1357, July 1994.

[18]. L.B. Pankratz, Thermodynamic properties of elements and oxides, US Department of Interior Bureau of Mines: Bulletin 672;1982

[19]. A.K. Niessen, F.R. de Boer, R. Boom, P.F. de Chatel, W.C.M. Mattens, and A.R. Miedema, Model predictions for the enthalpy of formation of transition metal alloys II, Calphad, vol. 7, pp. 51-70, 1983.

[20]. T.B. Massalski, P.R. Subramanian, H. Okamoto, L. Kacprzak (Eds.), *Binary Alloy Phase Diagrams*, 2nd ed., ASM, Materials Park: Ohio, 1990.

LnRhO$_3$	ΔG^0 Jmol^{-1}
LaRhO$_3$	$-70780 + 4.89(T/K)\ (\pm180)$
DyRhO$_3$	$-52710 + 3.821(T/K)\ (\pm182)$
GdRhO$_3$	$-56603 + 3.78(T/K)(\pm60)$
HoRhO$_3$	$-50535 + 3.85(T/K)\ (\pm78)$
TmRhO$_3$	$-46474 + 3.925\ (T/K)\ (\pm104)$
SmRhO$_3$ (cubic-Sm$_2$O$_3$)	$-60467 + 3.58(T/K)(\pm139)$
SmRhO$_3$ (Monoclinic-Sm$_2$O$_3$)	$-64230 + 6.97(T/K)(\pm75)$
NdRhO$_3$	$-66256 + 5.64(T/K)(\pm197)$
YbRhO$_3$	$-43164 + 3.436(T/K)(\pm130)$
PrRhO$_3$	$-67831 + 5.299(T/K)(\pm50)$

Table 1: Change in Standard Gibbs energy of formation for the reaction ½ Ln$_2$O$_3$ + ½ Rh$_2$O$_3$→LnRhO$_3$

| LnRhO$_3$	$\Delta H_f^0 (298.15\ K)$ kJ mol^{-1}	$S^0 (298.15\ K)$ J mol^{-1}K^{-1}
DyRhO$_3$	-1187.2±6.4	108.9±4.2
GdRhO$_3$	-1172.8±3.2	109.3±0.7
HoRhO$_3$	-1195.35±4.3	113.08±1.5
TmRhO$_3$	-1193.89±2.86	103.8±1.6
SmRhO$_3$	-1176.9±1.7	106.65±8.4
NdRhO$_3$	-1172.52±1.6	111.5±0.4
YbRhO$_3$	-1153±3	100.93±0.6
PrRhO$_3$	−67.81 ±0.115	108.89 ±1.3

Table 2: Thermodynamic properties of LnRhO$_3$ at 298.15 K [7-13,15].

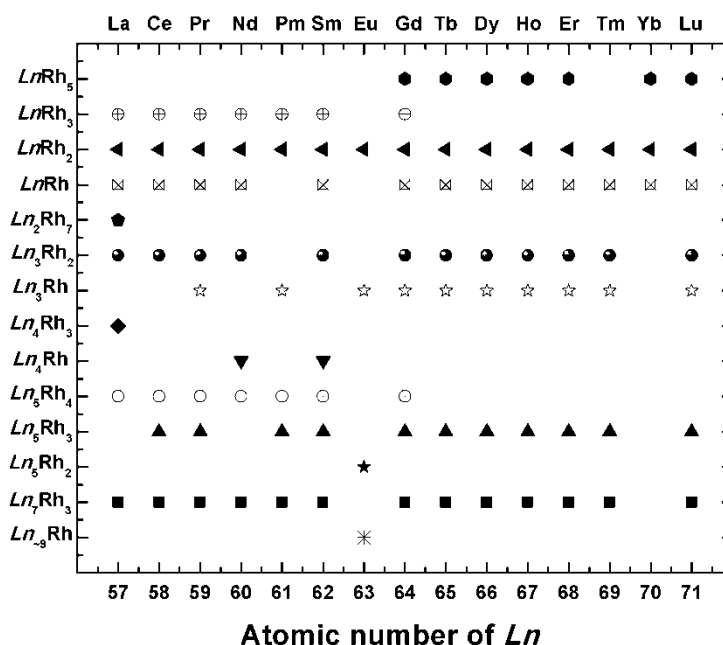| La-Rh-O system	Tm-Rh-O system	Nd-Rh-O system	Sm-Rh-O system
α-La+ La$_4$Rh$_3$+ La2O3	Tm + Tm$_3$Rh + Tm$_2$O$_3$	Nd + Nd−Rh (*l*) + Nd$_2$O$_3$,	Sm$_2$O$_3$ + SmRhO$_3$ + Rh
'La$_4$Rh$_3$'+La$_5$Rh$_4$ +La$_2$O$_3$	Tm$_3$Rh + Tm$_7$Rh$_3$ + Tm$_2$O$_3$	Nd−Rh (*l*)+Nd$_3$Rh$_2$+ Nd$_2$O$_3$	SmRhO$_3$ + Rh$_2$O$_3$ + Rh
La$_5$Rh$_4$ +LaRh+La$_2$O$_3$	Tm$_7$Rh$_3$ + Tm$_5$Rh$_3$ + Tm$_2$O$_3$	Nd$_3$Rh$_2$+ Nd$_5$Rh$_4$ + Nd$_2$O$_3$	'SmRh$_2$' + Rh + Sm$_2$O$_3$
LaRh+ LaRh$_2$'+ La$_2$O$_3$	Tm$_5$Rh$_3$ + Tm$_3$Rh$_2$ + Tm$_2$O$_3$	Nd$_5$Rh$_4$ + NdRh + Nd$_2$O$_3$	SmRh + 'SmRh$_2$' + Sm$_2$O$_3$
LaRh$_2$' + LaRh$_3$+La$_2$O$_3$	Tm$_3$Rh$_2$ + TmRh + Tm$_2$O$_3$	NdRh + 'NdRh$_2$'+ Nd$_2$O$_3$	Sm$_5$Rh$_4$ + Sm$_2$O$_3$
LaRh$_3$ +Rh +La2O3	TmRh + "TmRh$_2$" + Tm$_2$O$_3$	'NdRh$_2$'+ NdRh$_3$ + Nd$_2$O$_3$,	Sm$_7$Rh$_3$ + Sm$_5$Rh$_3$ + Sm$_2$O$_3$
La$_2$O$_3$ + Rh + LaRhO$_3$	"TmRh$_2$" + Rh + Tm$_2$O$_3$	NdRh$_3$ +Rh + Nd$_2$O$_3$	Sm$_4$Rh + Sm$_7$Rh$_3$ + Sm$_2$O$_3$
LaRhO$_3$ +Rh$_2$O$_3$ +Rh		Rh + Nd$_2$O$_3$ + NdRhO$_3$	Sm (s.s.) + Sm$_2$O$_3$
		Rh + NdRhO$_3$ + Rh$_2$O$_3$	Sm$_2$O$_3$ + SmRhO$_3$
			SmRhO$_3$ + Rh$_2$O$_3$

Table 3a: Experimentally obtained three-phase equilibria in Ln-Rh-O system [8, 10-12]

Dy-Rh-O	Gd-Rh-O	Ho-Rh-O	Yb-Rh-O system	Pr-Rh-O system	Ce-Rh-O system
$Dy + Dy_3Rh + Dy_2O_3$	$\beta\text{-Gd} + Gd(l) + Gd_2O_3$	$Ho + Ho_3Rh + Ho_2O_3$	$Rh_xYb_{1-x}(l) + RhYb + Yb_2O_3,$	$Pr(S) + Pr(i) + Pr_2O_3$	$Ce(l) + Ce_5Rh_4 + Ce_2O_3$
$Dy_3Rh + Dy_7Rh_3 + Dy_2O_3$	$Gd(l) + Gd_5Rh_3 + Gd_2O_3$	$Ho_3Rh + Ho_7Rh_3 + Ho_2O_3$	$RhYb + Rh_2Yb + Yb_2O_3$	$Pr(i) + Pr3Rh + Pr_2O_3$	$Ce_5Rh_4 + CeRh + Ce_2O_3$
$Dy_7Rh_3 + Dy_5Rh_3 + Dy_2O_3$	$Gd_5Rh + Gd_7Rh_3 + Gd_2O_3$	$Ho_7Rh_3 + Ho_5Rh_3 + Ho_2O_3$	$Rh_2Yb + Rh + Yb_2O_3$	$Pr_3Rh + Pr_7Rh_3 + Pr_2O_3$	$CeRh + \text{'}CeRh_2\text{'} + Ce_2O_3$
$Dy_5Rh_3 + Dy_3Rh_2 + Dy_2O_3$	$Gd_7Rh_3 + Gd_5Rh_3 + Gd_2O_3$	$Ho_5Rh_3 + Ho_3Rh_2 + Ho_2O_3$	$Rh + Yb_2O_3 + YbRhO_3$	$Pr_7Rh_3 + Pr_5Rh_3 + Pr_2O_3$	$\text{'}CeRh_2\text{'} + CeRh_3 + Ce_2O_3$
$Dy_3Rh_2 + DyRh + Dy_2O_3$	$Gd_5Rh_3 + Gd_5Rh_4 + Gd_2O_3$	$Ho_3Rh_2 + HoRh + Ho_2O_3$	$Rh + YbRhO_3 + Rh_2O_3$	$Pr_5Rh_3 + Pr_3Rh_2 + Pr_2O_3$	$CeRh_3 + Rh + Ce_2O_3$
$DyRh + DyRh_2 + Dy_2O_3$	$Gd_5Rh_4 + GdRh + Gd_2O_3$	$HoRh + HoRh_2 + Ho_2O_3$		$Pr_3Rh_2 + Pr_5Rh_4 + Pr_2O_3$	$Rh + Ce_2O_3 + Ce_3O_5$
$DyRh_2 + DyRh_5 + Dy_2O_3$	$GdRh + GdRh_2 + Gd_2O_3$	$HoRh_2 + HoRh_5 + Ho_2O_3$		$Pr_5Rh_4 + PrRh + Pr_2O_3$	$Rh + Ce_3O_5 + Ce_7O_{12}$
$DyRh_5 + Rh + Dy_2O_3$	$GdRh_2 + GdRh_3 + Gd_2O_3$	$HoRh_5 + Rh + Ho_2O_3$		$PrRh + PrRh_2 + Pr_2O_3$	$Rh + Ce_7O_{12} + CeO_{2-x}$
$Rh + Dy_2O_3 + DyRhO_3$	$GdRh_3 + Rh + Gd_2O_3$	$Rh + Ho_2O_3 + HoRhO_3$		$PrRh_2 + PrRh_3 + Pr_2O_3$	$Rh + CeO_{2-x} + Rh_2O_3$
	$Rh + C\text{-}Gd_2O_3 + GdRhO_3$	$Rh + Rh_2O_3 + HoRhO_3$		$PrRh_3 + Rh + Pr_2O_3$	
	$Rh + B\text{-}Gd_2O_3 + GdRhO_3$			$Rh + Pr_2O_3 + PrRhO_3$	
	$Rh + GdRhO_3 + Rh_2O_3$			$Rh + Rh_2O_3 + PrRhO_3$	
				$Pr_2O_3 + PrRhO_3 + Pr_7O_{12}$	

Table 3b: Three-phase equilibria in Ln-Rh-O system computed from thermodynamic data [6-7,9, 13-15]
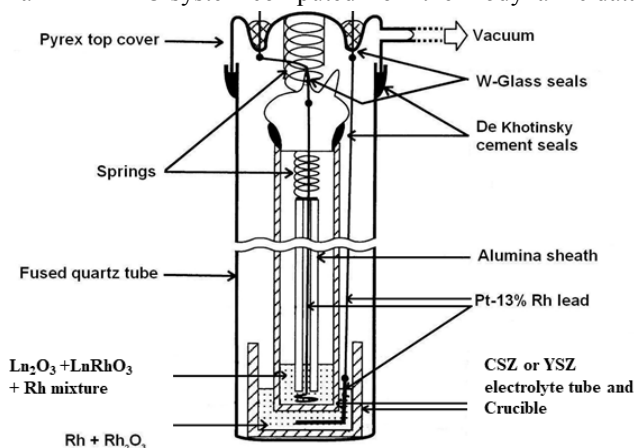
Fig. 1 Schematic diagram of the apparatus for the measurement of electromotive force (emf) of the solid-state electrochemical cell

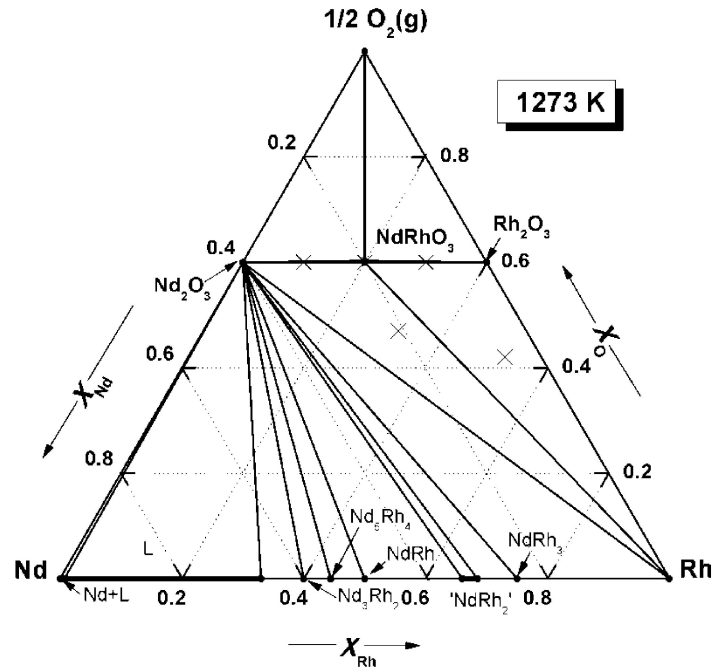**Fig. 2** Systematics of compounds in *Ln*-Rh binary systems

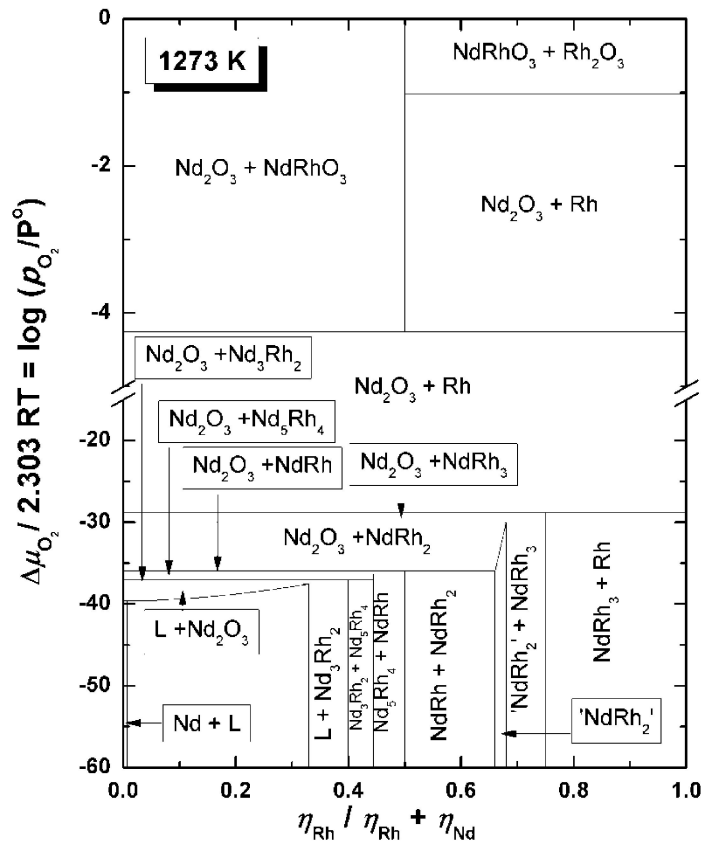**Figure 3** Ternary phase diagram of Nd-Rh-O system at 1273 K.

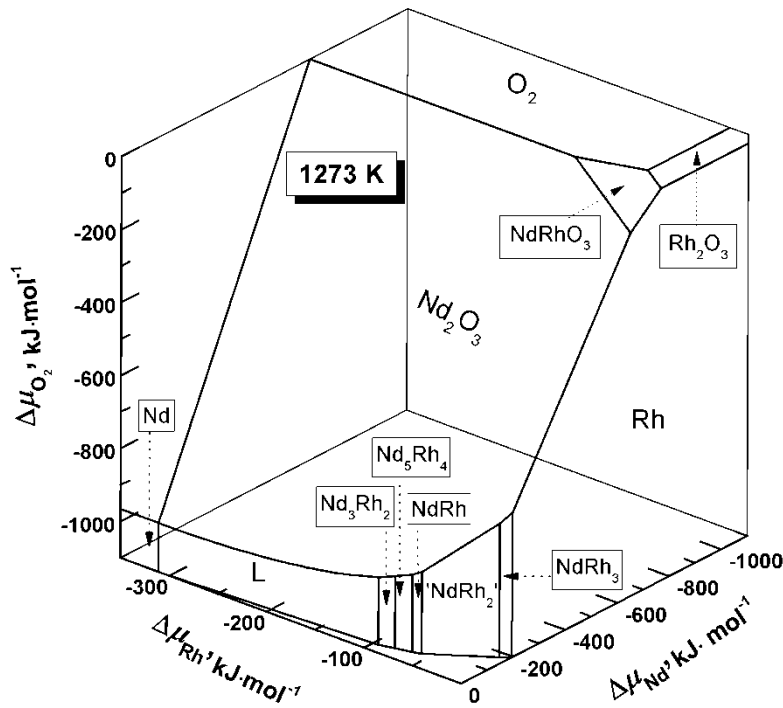**Figure 4** 2-Dimensional oxygen potential diagram of Nd-Rh-O system at 1273 K.

Figure 5 Three-dimensional chemical potential diagram of Nd-Rh-O system at 1273 K